Photoelectrical properties of semiconductor tips in scanning tunneling microscopy

M. W. J. Prins,* R. Jansen, R. H. M. Groeneveld, A. P. van Gelder, and H. van Kempen
Research Institute for Materials, University of Nijmegen, Toernooiveld 1, NL-6525 ED Nijmegen, The Netherlands
(Received 26 July 1995)

We describe a model as well as experiments on the electrical properties of a photoexcited tunnel junction between a metal and a semiconductor material, as is established in a scanning tunneling microscope. The model treats the case in which carrier transport is mediated by capture and relaxation in the semiconductor surface states. In the semiconductor, majority carrier transport is determined by thermionic emission over the Schottky barrier and subsequent surface recombination. By optical excitation an additional minority carrier current is generated. The voltage that develops on the semiconductor surface is determined by the balance between majority and minority carrier current in the semiconductor, and the current across the tunnel barrier. We present model calculations of the (nonplanar) band-bending profile in the semiconductor, which indicate that the subsurface electric field operates as an electrical lens that can focus or defocus the current. Measurements were performed with moderately doped GaAs tips or samples prepared by cleavage. Continuous as well as modulated photoexcitation was used. Relationships are determined between tunnel current, applied voltage, incident optical power, and tip-sample distance. The experimental results are well described by the model that includes carrier capture in the semiconductor surface states. It is shown that the sensitivity of the tunnel current to small variations in optical power is determined by the ratio of the tunnel barrier conductance to the Schottky barrier conductance. The implications for near-field optical imaging and spin-polarized tunneling with semiconductor tips are discussed.

I. INTRODUCTION

Since its invention, the scanning tunneling microscope (STM) (Ref. 1) has been used for studies on semiconductor materials. Initially, these studies were mainly concerned with the determination of the atomic arrangement at semiconductor surfaces, but soon thereafter the spectroscopic capabilities of the STM were applied in order to reveal information on the semiconductor energy bands.[2] From these investigations it appeared that the current flow through the semiconductor can seriously be affected by the STM-induced band bending in the semiconductor subsurface region, most notably with semiconductors of low doping density.[3]

When irradiating the semiconductor material with light, the produced electron-hole pairs are separated by the internal electric field of the band-bending region, in this way producing a surface photovoltage and the possibility to draw a current without applying an external voltage. Hence, the semiconductor band-bending profile influences the results of photoexcitation in a sensitive way. Photoexcited STM studies have been conducted with the semiconductor material as the sample,[4] but more recently also as a tip material photoexcited semiconductors have been subjected to investigation.[5–7] These tips hold special attraction with regard to near-field optical imaging[8] and as sources of optically oriented spin-polarized electrons.[9–11]

In this paper, we intend to develop a thorough understanding of the current transport properties of photoexcited semiconductor materials in the STM. The outline is as follows. First, we present a model on electrical transport in a photoexcited metal-semiconductor STM junction for continuous as well as modulated irradiation. The model includes the influence of surface states on the semiconductor surface. Thereafter, we show experimental data taken with moderately doped GaAs ($\sim 10^{23}\,\mathrm{m}^{-3}$) under ambient conditions. We present results on the relationship between tunnel current, applied voltage, incident power, tip-sample distance, and sensitivity to small variations in light power. The results are compared with our model calculations. Finally, we draw conclusions on the internal transport mechanisms in our junctions, and discuss the consequences for the usage of optically excited semiconductor tips in a STM.

II. ELECTRO-OPTICAL MODEL

For more than a century, the electrical properties of metal-insulator-semiconductor junctions have been investigated in view of their rectifying behavior and photonic applications (for excellent textbooks see Refs. 12–14). These investigations were mainly concerned with solid-state junctions having a planar geometry. Model calculations on semiconductor devices are complicated by the fact that electrostatic effects (band-bending) and carrier transport (electron distribution function, electrochemical potential) are strongly coupled. In addition, transport of majority as well as minority carriers has to be considered. In order for the calculations to be tractable, usually important assumptions are made. In devices with a very thin insulating layer that is of negligible resistance, one can assume that the semiconductor surface is in equilibrium with the metallic electrode. When the insulating layer strongly inhibits the current flow, one may assume that the semiconductor surface is in equilibrium with the semiconductor bulk. In a STM, the conductance of the tunnel junction is an adjustable parameter; often we cannot use one of the above limiting cases, and a more general treatment is required.

In Sec. II A, we will present a model for current flow in a photoexcited metal-semiconductor tunnel junction, where now the surface electrochemical potential is a free parameter. The main assumption underlying this model is that the current flows via the surface states on the semiconductor sur-

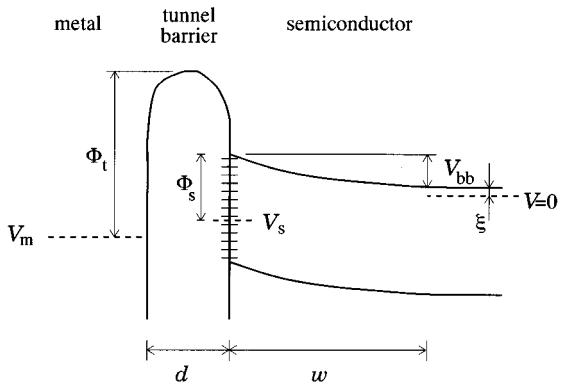

FIG. 1. One-dimensional electronic energy diagram of a tunnel junction between a metal and a semiconductor. Indicated are the tunnel barrier height (Φ_t), the Schottky barrier height (Φ_s), the band-bending voltage (V_{bb}), the difference between the Fermi level and majority carrier band edge in the semiconductor bulk (ξ), the voltage applied between the metal and the semiconductor bulk (V_m), and the semiconductor surface electrochemical potential (V_s). Along the vertical axis, the parameters are defined in volts. The metal-to-semiconductor separation (d) and the depth of the band-bending region (w) are indicated horizontally. The picture is not on scale, because, in general, w is more than an order of magnitude larger than d.

face, instead of directly from the metal into the semiconductor conduction or valence band. The incorporation of surface states into a model description is particularly important when considering semiconductor tips, because at the tip apex surface states are present due to the strongly reduced crystallographic symmetry (so even in a well-controlled environment). Another important consideration stems from the fact that in a STM the dimensions of the tunnel barrier are far smaller than the typical depth of the band-bending region in the semiconductor. Due to this fact, the profile of the band-bending region will strongly deviate from planar symmetry. In Sec. II B, we will present calculations of the band-bending region in a semiconductor material, for the case that a tunnel junction is established on a planar semiconductor sample, as well as for the case of a semiconductor shaped as a tip. Finally, in Sec. II C, we will present a quasi-one-dimensional model for direct as well as displacement currents resulting from modulated photoexcitation.

A. Planar junction

In a metal-semiconductor tunnel junction, a metallic and a semiconducting material are separated by a tunnel barrier. Due to work function differences, surface charges and the application of voltage to the junction, a space charge layer (depletion layer) is generally formed in the semiconductor subsurface region. Hence we are confronted with a serial arrangement of two barriers: a tunnel barrier and a so-called Schottky barrier. In Fig. 1, we have drawn the one-dimensional energy diagram for a planar tunnel junction with an n-type semiconductor. Indicated are the conduction and valence band edges in the semiconductor bulk, the band-bending region in the semiconductor, the surface states on the semiconductor surface, the tunnel barrier, and the metallic counter electrode. The bulk of the semiconductor is at zero electrical potential, the metallic electrode at the externally applied voltage V_m. The so-called surface or interface states within the forbidden energy gap are caused by the reduced symmetry of a surface as compared with the bulk, or by a modified chemical composition at the surface. For example, under ambient conditions GaAs forms a noncrystalline native oxide with a high density of surface states and a thickness of about a nanometer.[15] At the semiconductor surface, we have indicated the surface electrochemical potential V_s. This potential can properly be assigned if the surface carriers are in thermal equilibrium. Because currents are flowing in the junction, strictly speaking this assumption is invalid. But since the processes of carrier capture and relaxation are generally very efficient at surfaces with surface states,[16] we presume that the occupancy of the surface states obeys the Fermi-Dirac distribution. As can be seen from the figure, the total band bending in the space charge region is given by

$$V_{\mathrm{bb}}=\Phi_s-V_s-\xi, \tag{1}$$

where Φ_s is the electrostatic Schottky barrier height (in volts), and ξ is the difference between the Fermi level and the majority carrier band edge in the semiconductor bulk. Φ_s is defined as the difference between the surface quasi-Fermi level and the position of the majority carrier band edge at the semiconductor surface. In the following, we will assume that $|V_{\mathrm{bb}}|\gg k_BT/e$, and that the surface quasi-Fermi level remains between the conduction and valence band edges at the surface.

Schottky majority carrier flow. Concerning majority carrier transport through the Schottky barrier, we will limit the model to the case where the dominant transport mechanism is given by thermally assisted emission of majority carriers over the barrier and subsequent recombination at the surface (the notions of majority and minority carriers refer to the carrier types as encountered in the semiconductor bulk). For high-mobility semiconductors this is not a very strong limitation. For example, at room temperature majority carrier transport in GaAs Schottky barriers is dominated by this so-called thermionic emission at doping densities of the order $10^{23}\,\mathrm{m}^{-3}$ or lower. Following the thermionic emission theory, the density of current J_s flowing from the semiconductor surface to the bulk is given by[12–14]

$$J_s=J_0[\exp(\beta V_s)-1\,],\quad J_0\equiv qNv_r\exp(-\beta\Phi_s), \tag{2}$$

where J_0 is the saturation current density, N is the semiconductor doping density, v_r is the effective recombination velocity at the potential energy maximum of the barrier, and $\beta=q/k_BT$. Here, k_B is the Boltzmann constant, and T is the temperature. The parameter q equals $+e$ if the energy bands are bending upward toward the surface (as in Fig. 1) and $-e$ if the bands are bending downward, where e is the absolute magnitude of the electronic charge. In most n-type semiconductors the energy bands are bending upward toward the surface, such that $\Phi_s>0$, $\xi>0$, and $q=+e$; in most p-type materials the bands are bending downward and these three parameters are negative. The exponential factors in Eq. (2) cause the well-known rectifying current-voltage characteristic of a Schottky diode: if $\beta V_s>0$, the band-bending magnitude is decreased and the Schottky barrier is operated

in forward bias, whereas if $\beta V_s<0$, the band bending is increased and the diode is reversely biased. In case the actual process of thermionic emission is limiting the majority carrier transport (as in metal-capped Schottky diodes without a tunnel barrier), the effective recombination velocity is given by $A^{**}T^2/[eN]$, where A^{**} is the modified Richardson constant.[12] For example, in a metal-GaAs Schottky diode of $10^{23}\,\mathrm{m}^{-3}$ doping density, the effective recombination velocity is of order $10^7\,\mathrm{ms}^{-1}$. At free or oxidized semiconductor surfaces, the recombination is generally less efficient, implying that surface recombination instead of thermionic emission limits the current flow. The surface recombination velocity is of order $10^5\,\mathrm{ms}^{-1}$, for example, in the native oxide on GaAs.[16] Finally, Schottky barrier characteristics can deviate from the predictions of the thermionic emission theory, due to the importance of other transport mechanisms, for example, thermally assisted field emission or tunneling through the barrier. These transport mechanisms can be incorporated by adopting a slightly modified thermionic emission equation:[14]

$$J_s=J_0\exp(\beta V_s/n)[1-\exp(-\beta V_s)], \tag{3}$$

where n is the ideality factor.[17] With $n=1$, we recover Eq. (2); with $n>1$, the Schottky diode rectification is diminished. This formula determines the potential V_s required to draw a current through the Schottky barrier. As we will see later, V_s can have an appreciable value when using typical STM currents.

As pointed out in the previous equations, the majority carrier current through the Schottky barrier depends on the Schottky barrier height (Φ_s) via the formula for J_0. In case of a limited density of surface states, the barrier height is not constant due to capacitive interactions. To first order in V_m and V_s, the Schottky barrier height is easily deduced to be given by

$$\Phi_s=\Phi_s^0-\frac{\tilde{C}_t[V_m-V_s]-\tilde{C}_sV_s}{\tilde{C}_t+\tilde{C}_s+e^2D_{\mathrm{ss}}}\equiv\Phi_s^0-\gamma_t[V_m-V_s]+\gamma_sV_s,$$

$$0\leqslant\gamma_{t,s}\leqslant1, \tag{4}$$

where Φ_s^0 is the barrier height in the equilibrium state (when $V_m=V_s=0$), $\tilde{C}_t$ is the tunnel barrier capacitance per unit area, $\tilde{C}_s$ is the Schottky barrier capacitance per unit area, and D_{ss} is the density of surface states (units $\mathrm{m}^{-2}\,\mathrm{J}^{-1}$).[18] The tilde ($\tilde{}$) denotes that the capacitances are defined per unit area. The γ factors are defined as $\gamma_t\equiv\tilde{C}_t/[\tilde{C}_t+\tilde{C}_s+e^2D_{\mathrm{ss}}]$, and $\gamma_s\equiv\tilde{C}_s/[\tilde{C}_t+\tilde{C}_s+e^2D_{\mathrm{ss}}]$. Higher order terms to Eq. (4) result from the fact that $\tilde{C}_s$ and D_{ss} are not truly constant.[19] Equation (4) tells us how at the surface the position of the majority carrier band-edge shifts with respect to the surface quasi-Fermi level, in response to the drop of electrochemical potential across the tunnel barrier (weighted by the factor γ_t) and in response to the potential drop across the Schottky barrier (weighted by the factor γ_s). The surface Fermi level is said to be pinned if γ_t and γ_s are approximately zero, i.e., in the case of a high density of surface states. Combining Eqs. (1) and (4), the expression for the total band-bending becomes

$$V_{\mathrm{bb}}=V_{\mathrm{bb}}^0-\gamma_tV_m-[1-\gamma_t-\gamma_s]V_s\ \text{ with }\ V_{\mathrm{bb}}^0=\Phi_s^0-\xi. \tag{5}$$

The first term (V_{bb}^0) represents the band bending in the equilibrium state. The second term describes the dependence of the band bending on the external bias (V_m). In case of a limited density of surface states, the semiconductor subsurface region is not completely shielded from the metal, such that the applied bias influences the band bending in the semiconductor by a capacitive coupling.[3,19,20] The third term takes account of the band bending caused by the drop of electrochemical potential across the Schottky barrier (V_s), that is nonzero only in case of current flow in the semiconductor. The prefactor $[1-\gamma_t-\gamma_s]$ equals zero if there are no surface states ($D_{\mathrm{ss}}=0$), because in that case no charge is induced at the semiconductor surface. In order to determine the importance of these effects in our experiment, we need to assess the values of the weight factors γ_t and γ_s, which are a function of $\tilde{C}_s$, $\tilde{C}_t$, and D_{ss}. The capacitance of a Schottky barrier is associated with the modification of the depth of the space charge region upon change of the band bending. In the depletion approximation (assuming a constant density of space charge eN) the capacitance per unit area is[12–14]

$$\tilde{C}_s=\epsilon_0\epsilon_s/w,\quad w=\sqrt{2\epsilon_0\epsilon_sV_{\mathrm{bb}}/eN}, \tag{6}$$

where w is the depth of the depletion region. In our experiments, w ranges from 50 to 100 nm, so that (with $\epsilon_s=13$) $\tilde{C}_s$ ranges between 1 and $2\times10^{-3}\,\mathrm{Fm}^{-2}$. For $\tilde{C}_t$, we can use the planar capacitor formula $\tilde{C}_t=\epsilon_0\epsilon_t/d$, where d is the separation between the metal and the semiconductor surface. For a vacuum tunnel barrier ($\epsilon_t=1$) with $d=1$ nm, $\tilde{C}_t\simeq9\times10^{-3}\,\mathrm{Fm}^{-2}$. Finally, the density of surface states (D_{ss}) ranges between 10^{36} and $10^{37}\,\mathrm{m}^{-2}\,\mathrm{J}^{-1}$ for oxidized GaAs.[12,15] From the above values, we estimate γ_t to range between 0.05 and 0.3, and find that γ_s is nearly an order of magnitude smaller than γ_t in our experimental situation. The γ factors are rather small due to the high density of surface states present in the native oxide on GaAs. With the estimated γ factors, we conclude that in our experiments the band bending in the semiconductor [cf. Eq. (5)] is most strongly determined by the surface electrochemical potential, and is to a lesser extent sensitive to the potential of the metallic electrode.

Photoexcited minority carrier flow. Electron-hole pairs can be generated in the semiconductor material by irradiation with photons of energy higher than the band gap. From the bulk of the semiconductor, the carriers can reach the space charge region by diffusion. In the space charge region, the minority carriers are swept toward the surface by the internal electric field,[21] creating a photocarrier current from the semiconductor surface toward the bulk of size J_p per unit area. J_p is determined by many parameters, such as the incident light power P, the fraction of the light power that is absorbed in the semiconductor f_{abs} ($0\leqslant f_{\mathrm{abs}}\leqslant1$), and the extent to which the processes of minority carrier diffusion and drift are effective in collecting photocarriers at the semiconductor surface. This collection efficiency η_c ($0\leqslant\eta_c\leqslant1$) depends on the absorption depth of the light relative to the bulk diffusion length and the depth of the space charge region. Solving the diffusion equation in case of planar symmetry yields[22]

$$\eta_c = 1 - \frac{\exp(-\alpha_{\rm ph} w)}{\alpha_{\rm ph} L_d + 1}, \tag{7}$$

where $\alpha_{\rm ph}$ is the photon absorption coefficient, and L_d is the minority carrier diffusion length. The diffusion length is given by $L_d = [k_B T/e\ \mu\tau]^{1/2}$, where μ is the minority carrier mobility and τ is the minority carrier lifetime.[16] In high-quality GaAs, the electron and hole mobility are about 0.8 and 0.04 $\mathrm{m^2\,V^{-1}\,s^{-1}}$, respectively. The minority carrier lifetime depends on the majority carrier density (so on doping density and temperature) and on the material quality. At room temperature, the minority carrier lifetime is a few nanoseconds in moderately doped GaAs,[16] so the diffusion length ranges between one and a few micrometers. For photons of 633 nm wavelength $\alpha_{\rm ph} = 4\times 10^6\ \mathrm{m^{-1}}$, i.e., the optical penetration depth is 250 nm.[23] In other words, η_c is close to unity, and is modified by less than 4% when w increases from 50 to 100 nm. Hence, we assume η_c to be constant for our experiment. This leads to the following equation for the photocurrent density flowing from the semiconductor surface toward the bulk:

$$J_p = -f_{\rm abs}\eta_q \eta_c \frac{qP}{E_{\rm ph} A_l}, \tag{8}$$

where η_q is the quantum efficiency of conversion of photons to electron-hole pairs ($0 \leqslant \eta_q \leqslant 1$), $E_{\rm ph}$ is the energy per photon, and A_l is the illuminated area. In our experiments, the light intensity P/A_l ranges between zero and $10^6\ \mathrm{Wm^{-2}}$. The total efficiency $\eta_q \eta_c$ can be close to unity for many semiconductor materials.[24] As we have seen, the space charge region in the semiconductor represents a barrier for majority carrier transport (J_s). On the other hand, it constitutes an accelerating field for photoexcited minority carriers (J_p). Note that the sign of J_p is fixed by the sign of q, i.e., by the direction of the band bending. It is interesting to estimate the excess minority carrier concentration at the surface ($N_{\rm sr}$) that is associated with the surface recombination current due to photoexcited carriers. Given the surface recombination velocity $v_{\rm sr}$, the density of surface recombination current becomes $J_{\rm sr} \simeq e v_{\rm sr} N_{\rm sr}$. In our experiments, the maximum photocurrent density is of order $10^6\ \mathrm{Am^{-2}}$. Using $v_{\rm sr} = 10^5\ \mathrm{ms^{-1}}$, we find that $N_{\rm sr} \leqslant 10^{20}\ \mathrm{m^{-3}}$. This carrier concentration is negligible compared to the semiconductor doping density in our experiments ($\sim 10^{23}\ \mathrm{m^{-3}}$), and also too small to cause any significant minority carrier diffusion from the surface back into the bulk.

Tunneling current. The current across the tunnel barrier depends on the tunnel barrier shape, and on the electronic structure of the metal and of the semiconductor surface. Since these properties are not known in detail, we adopt the following simple description. The most characteristic property of a tunnel barrier is that the tunneling current has an exponential dependence on electrode separation. If the voltage drop across the tunnel barrier ($V_m - V_s$) is far smaller than the tunnel barrier height, the tunnel current density (J_t) becomes[25]

$$J_t \propto \exp(-2\kappa d)[V_m - V_s], \quad \kappa = [\,2 m_e e \hat{\Phi}_t/\hbar^2]^{1/2}, \tag{9}$$

where m_e is the electron mass, and d is the electrode separation; in a STM, d is of the order of one nm.[26] $\hat{\Phi}_t$ is the so-called apparent barrier height that equals the barrier height (Φ_t) in case of a tunnel barrier with a rectangular shape.[25] Under ambient conditions, the apparent barrier height is generally lower than one volt, due to surface contamination.[25] In our experiments the voltage drop ($V_m - V_s$) is also of the order of one volt, which gives rise to nonlinear current-voltage characteristics. In our model description this can be accounted for by adding a cubic term to the voltage dependence of the current.[27]

The above description is valid if the surface electronic structures of both the metal and the semiconductor are not strongly dependent on the energy. With regard to the semiconductor, this translates into the requirement that the tunneling occurs from a continuous distribution of surface states, rather than from the semiconductor conduction or valence band. By a simple argument, we can estimate whether this requirement is fulfilled. The probability of carrier capture in surface states is given by $\sigma_{\rm cap} N_{\rm cap}$, where $\sigma_{\rm cap}$ is the capture cross section and $N_{\rm cap}$ is the density of active surface states. Using $N_{\rm cap} \simeq 10^{17}$–$10^{18}\ \mathrm{m^{-2}}$ for the GaAs native oxide[12,15] and $\sigma_{\rm cap} \simeq 10^{-19}$–$10^{-18}\ \mathrm{m^2}$ from Ref. 28, we obtain a capture probability between 0.01 and unity. This is several orders of magnitude higher than the carrier transmission probability through a typical tunnel barrier;[26] thus, we may assume that the tunnel current flows through the surface states instead of directly from the semiconductor conduction and valence bands into the metallic electrode (this issue is addressed more rigorously in Ref. 29).

Let us consider the special case that $J_t = 0$ because $V_m = V_s$. At that point V_m is equal to the open-circuit voltage or so-called surface photovoltage (SPV), which is determined by the balance of majority and minority carrier current in the semiconductor: $J_s + J_p = 0$. Using Eqs. (3), (4), and $\beta V_s \gg 1$, we find

$$\mathrm{SPV} = \frac{n}{1-\gamma_s n}\beta^{-1}\ln(-J_p/J_0^0), \quad J_0^0 \equiv qNv_r \exp(-\beta\Phi_s^0), \tag{10}$$

Since J_p is proportional to the optical power P, a measurement of the SPV versus P can serve to determine the applicability of the presented model.

B. STM junction

The semiconductor surface electrostatic potential [i.e., the band-bending voltage given in Eq. (5)] is a function of (i) the electric field between the semiconductor and the metallic electrode, and (ii) the surface electrochemical potential. The first effect is only important in case of a limited density of surface states, because otherwise the semiconductor subsurface region is completely shielded from the metal by the surface states [cf. the term with V_m in Eq. (5)]. The second mechanism is only effective in case of a nonzero density of surface states, otherwise charge cannot be accommodated at the semiconductor surface [cf. the term with V_s in Eq. (5)]. If we establish a metal-semiconductor tunnel junction in an STM, (i) a nonuniform pattern of field lines is set up between the tip and the sample, and (ii) a nonuniform surface electrochemical potential is created. The latter results from the fact that the tunneling point represents a nanometer-sized injection point from which the current spreads out inside the

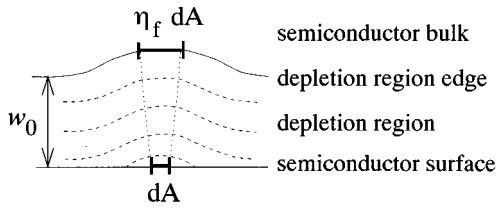

FIG. 2. Schematic outline of the depletion region in a planar semiconductor when a nonuniform reverse potential is applied to the surface. The dashed lines represent equipotential lines. The depletion field focusing efficiency (η_f) describes how, by following the electric field lines (represented by the dotted lines), an infinitesimal area dA is mapped onto an area η_f dA at the edge of the depletion region. In this case η_f is larger than unity, implying that the field lines are focusing toward the semiconductor surface.

semiconductor material. In other words, due to the nonplanar geometry of an STM, the generated band-bending profile will deviate from one-dimensional symmetry. A complete picture of the photoelectrical properties of such a system requires simultaneously solving the three-dimensional electrostatic and transport equations. The transport equation should include thermionic emission for the majority carriers, and diffusion (outside the depletion region) and drift (inside the depletion region) for the photoexcited minority carriers. Since this is not feasible, in the following we will develop a qualitative understanding of transport properties from electrostatic calculations only. The influence of the free carrier density associated with the tunneling current is neglected.[30]

Nonuniform band bending in a planar semiconductor. Let us consider a STM junction between a metallic tip and a planar semiconductor surface at $z = 0$, where now the nonuniform surface electrostatic potential is given by

$$\Phi(x,y,0) = F_0 + F_1(x,y), \tag{11}$$

where F_0 is the constant potential of the unperturbed semiconductor surface, and F_1 represents the relative potential perturbation locally caused by the tunnel junction (for these calculations it is immaterial which mechanism is causing the nonuniform surface potential). With this boundary condition, the subsurface depletion field has been calculated[31] using perturbation theory. The calculations show that, with a locally applied reverse potential ($F_1/F_0 > 0$), the depth of the space charge region is locally increased and that the field lines tend to focus toward the spot where the local potential is applied (cf. Fig. 2). With a forward potential ($F_1/F_0 < 0$), the field lines defocus toward the spot where the potential is applied. In other words, the local potential modifies the depth of the space charge region and generates a *lateral* component of the electric field in the semiconductor subsurface region. Concerning carrier transport, this results in an effective transport section that depends on the band-bending profile. In case of photoexcited minority carriers — which are accelerated along the field lines in the space charge region — the effective section is increased (decreased) with a locally increased (decreased) band bending. As such, the space charge field operates like an electrical lens with a variable diameter and focal length. Also the majority carrier transport is sensitive to the shape of the band-bending profile: the effective section for majority carrier transport will be larger with a reverse than with a forward potential. This effect may also provide an explanation for the weak rectification of current-versus-voltage characteristics often observed in point contacts on semiconductors.[13]

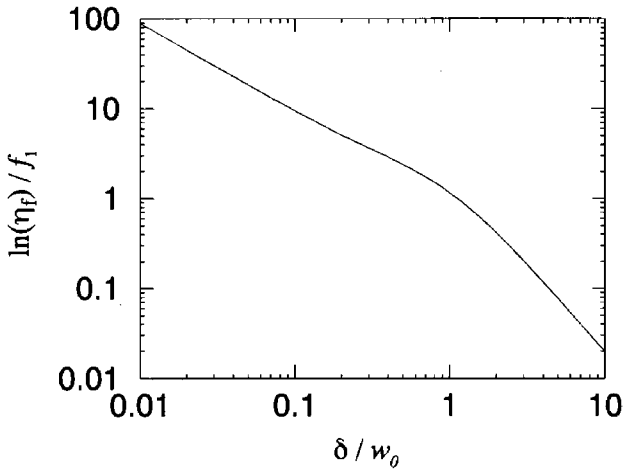

FIG. 3. The natural logarithm of the depletion field focusing efficiency (η_f) divided by the relative magnitude of the potential perturbation (f_1), drawn as a function of the Gaussian width of the potential perturbation (δ). δ is normalized to the depth of the depletion region in an unperturbed planar semiconductor material (w_0). The focusing efficiency was deduced from a depletion field calculation in a *planar* semiconductor material. The calculation (cf. Ref. 31) was performed to first order in the relative perturbation amplitude f_1.

In order to quantify the focusing properties of the depletion field, let us consider a potential perturbation of Gaussian shape:

$$F_1 = f_1 F_0 \exp(-r^2/\delta^2), \quad r = [x^2 + y^2]^{1/2}, \tag{12}$$

where δ is the Gaussian width and f_1 is the relative amplitude. We then calculate[31] the minority carrier trajectories in the depletion field and deduce a so-called focusing efficiency η_f. This efficiency describes how, by following the field lines, an infinitesimal area dA at $\vec{r} = \vec{0}$ is mapped onto an area η_f dA at the edge of the depletion region (cf. Fig. 2). From the calculations it follows that η_f exponentially depends on the perturbation amplitude f_1; the results are summarized in Fig. 3. For $f_1 > 0$ (reverse potential), the efficiency is larger than unity (focusing of field lines), whereas for $f_1 < 0$ (forward potential) the efficiency is smaller than unity (defocusing of field lines). Note that an increase of w_0 results in a larger focusing in a reverse bias operation, and results in a larger defocusing in a forward bias operation.

In our experiments, the depth of the unperturbed depletion region ranges between 50 and 100 nm. The magnitude of the Gaussian width (δ) follows from the exact mechanism causing the nonuniform surface potential. If it is the penetration of field lines from the metallic tip, δ is expected to be of the order of the tip radius. On the other hand, if the nonuniform surface electrochemical potential is the driving mechanism, δ will depend on the details of the current flow in the semiconductor subsurface region. When δ is larger than the depth of the unperturbed depletion region ($\delta \gg w_0$) the efficiency tends to unity, because in that limit the depletion field is

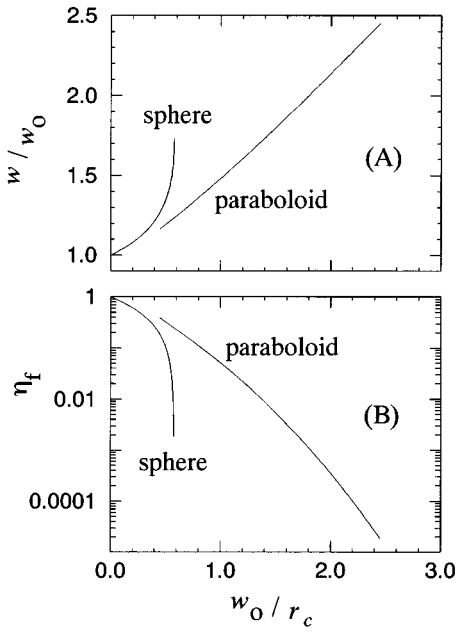

FIG. 4. (a) The depth of the depletion region (w) and (b) the depletion field focusing efficiency (η_f), as a function of the inverse of the radius of curvature (r_c^{-1}) of a semiconductor material. Results are indicated for a semiconductor sphere with radius r_c, as well as for a paraboloid semiconductor tip with a radius of curvature r_c at the apex. w_0 is the depth of the depletion region in an unperturbed planar semiconductor material (w_0). In all cases, a *constant surface potential* was assumed. The results for the sphere were derived from an exact calculation; the data for the paraboloid originate from an approximate solution (cf. Ref. 31).

nearly uniform. On the other hand, for a perturbation that is applied very locally ($\delta \ll w_0$), the depletion field profile is strongly nonplanar, such that η_f deviates from unity. The focusing efficiency can attain very large values in the case of a reverse bias potential and a small δ. Let us estimate a reasonable maximum for the focusing efficiency. A lower limit to δ is given by the fact that the electric field along the surface cannot exceed the dielectric breakdown field, which is close to 10^8 Vm^{-1} in GaAs;[12] taking a perturbation amplitude of 0.2 V, we find that δ is larger than 2 nm. Using $w_0 \simeq 100$ nm, the lower limit for the ratio δ/w_0 is 0.02. From Fig. 3 and taking $f_1=0.2$, we deduce that $\ln(\eta_f) \simeq 0.2\times 30$, i.e., a maximum depletion field focusing efficiency (η_f) of 4×10^2.

Band bending in a semiconductor tip. When the STM tip is of semiconductor material, its nonplanar geometry results in a nonplanar space charge field. This geometry is modeled in our calculation of the depletion field by assuming a rotationally symmetric body with a constant surface potential.[31] Figure 4 shows the calculated results for a semiconductor material of spherical symmetry, and for a semiconductor tip shaped as a paraboloid. Figure 4(a) depicts the depth of the depletion region as viewed along the symmetry axis (w), divided by the value for a planar semiconductor (w_0). As expected, the curves tend to unity for blunt tips ($r_c^{-1} \to 0$). In a convexly shaped semiconductor (i.e., for finite r_c), the depth of the depletion region is larger than in a planar semiconductor. For the sphere, the curve ends at $w=r_c=\sqrt{3}w_0$, for which the whole sphere has become depleted. The depth of the depletion region is not limited in a paraboloid semiconductor tip, because its shaft is of infinite length. For sharp paraboloid tips ($r_c < w_0$) the depth of the depletion region is proportional to the inverse of the radius of curvature. Figure 4(b) shows the focusing efficiency for the sphere and the paraboloid. The focusing efficiency equals unity for blunt tips and rapidly decreases for sharper tips, indicating that the field lines are defocusing toward the surface. The strong similarity of the curves in Figs. 4(a) and 4(b) stems from the fact that, for the considered range of parameters, the curvature of the equipotential lines in the depletion region closely resembles the curvature of the contour of the tip. In conclusion, when a tip-shaped semiconductor is compared to a planar semiconductor of the same material and with the same surface potential, the depletion region depth is larger and the focusing properties of the depletion field are biased toward defocusing.

Nonplanar carrier flow. The previous calculations demonstrate that the profile of the band bending region can strongly deviate from planar symmetry, when a metal-semiconductor tunnel junction is established in an STM. The driving mechanisms are the capacitive coupling between the tip and the sample, the nonuniform electrochemical potential at the semiconductor surface, and the shape of the tip. The most important conclusion is that we expect the flow of minority and majority carriers in the semiconductor to deviate from a one-dimensional picture. As an extension to our one-dimensional modeling of Sec. II A, we therefore introduce an effective semiconductor transport section $A_s = \pi R_s^2$, where R_s is the effective section radius. Model calculations can now be based on the following equations: $I_p = A_s J_p$, and $I_t = I_s + I_p$, where I_t is the tunneling current, I_s, is the Schottky barrier majority carrier current, and I_p, is the photocarrier current. As an interesting example, let us consider the situation that no external bias is applied ($V_m = 0$). In that case, the measured tunnel current cannot be larger than the photoexcited minority carrier current density multiplied by the effective transport section: $|I_t| \leqslant A_s |J_p|$. Substituting this inequality into Eq. (8) gives

$$A_s \geqslant \frac{|I_t| E_{\mathrm{ph}} A_l}{f_{\mathrm{abs}} \eta_q \eta_c |q| P} \quad \text{if} \quad V_m = 0. \tag{13}$$

In this way, a measurement of the magnitude of the tunnel current at $V_m = 0$ yields a minimum collection area that has had to be effective in the semiconductor in order to generate the measured tunnel current. In the limit of very small tip-sample separation, the semiconductor surface potential drops to zero and the tunneling current equals the photocurrent. In other words, if $V_m = V_s = 0$, the above inequality becomes an equality, yielding the true value for the effective section in that particular limit.

In our experiments, it is not possible to determine the effective transport section for the majority carriers, because the Schottky barrier height (which determines J_s) is not *a priori* known. As a first approximation, for the majority carriers we use the same effective section as is used for the minority carriers: $I_s = A_s J_s$. In reality this assumption is not very accurate, since the two carrier types follow different transport mechanisms (thermionic emission for majority carriers, diffusion and drift for minority carriers). However, an

error in the estimated majority carrier transport section of a factor of 10, for example, will limit the resulting error in the value of the Schottky barrier height (Φ_s) to $\sim \ln(10) k_B T/e \simeq 60$ mV, as we can read from Eq. (2).

C. Modulated photoexcitation

In the previous subsection, we have described the considerations that led to a modified one-dimensional model for direct current transport between a metal and a semiconductor material in a STM. The major result is that, although the tunnel current is led through a nanometer-sized constriction, in the semiconductor the electrostatic and electrochemical potential are modified over an area that can be considerably larger. When modulated photoexcitation is applied, in addition to the direct currents the displacement currents also have to be analyzed. Direct currents are driven by a drop of electrochemical potential, whereas displacement currents are caused by a drop of electrostatic potential. Let us assume a time-dependent surface electrochemical potential of the form $V_s(t) = \mathrm{Re}\{V_s + \Delta V_s \exp(j\omega t)\}$, while keeping V_m constant. As a result, through the Schottky barrier, a modulation of direct current density of size $\tilde{G}_s \Delta V_s$ is generated, where $\tilde{G}_s = \partial J_s / \partial V_s$ is the differential conductance per unit area derived from Eqs. (2)–(4). In addition, a displacement current density is generated with magnitude $j\omega \tilde{C}_s[\Delta V_s - \Delta \Phi_s] = j\omega \tilde{C}_s[1 - \gamma_t - \gamma_s]\Delta V_s$, where we have used Eq. (4) with $\Delta V_m = 0$. The factor $[1 - \gamma_t - \gamma_s]$ ranges between zero ($D_{ss} = 0$) and unity ($D_{ss} \to \infty$). Thus, a limited density of surface states causes a reduction of the displacement current when expressed in terms of the electrochemical potential. In this particular case, the reduction can be taken into account by an effective capacitance of size $\tilde{C}_s[1 - \gamma_t - \gamma_s]$. Due to the high density of surface states in the native oxide on GaAs, the γ factors are small in our experiments [cf. Eq. (6)]. Therefore, the reduction factor is not of great concern. Omitting the reduction factor, we describe the total modulation of Schottky barrier current density by a complex admittance per unit area $\tilde{Y}_s = \tilde{G}_s + j\omega \tilde{C}_s$, such that $\Delta J_s = \tilde{Y}_s \Delta V_s$.

Figure 5 shows the equivalent electrical circuit for time-dependent current transport in a metal-semiconductor STM junction, illuminated over an area $A_l > A_s$. Quite arbitrarily, the tip has been chosen to be the semiconductor material. Adopting a quasi-one-dimensional model, two parallel current transport channels are distinguished. The first, called the constricted current channel, accounts for the carrier flow through the semiconductor effective section A_s and the tunnel barrier admittance Y_t. The second, named the wide channel, describes current flow through the remaining illuminated part of the semiconductor with section $[A_l - A_s]$. The wide channel is capacitively coupled to the metallic electrode, described by a stray capacitance C_{str}. In the model, $Y_{s,c} = A_s \tilde{Y}_s$ refers to the Schottky admittance in the constricted channel, and $Y_{s,w} = [A_l - A_s]\tilde{Y}_s$ indicates the Schottky admittance in the wide channel. For completeness, also the external circuit admittance Y_{ex} has been incorporated in the figure. In the following analysis this parameter is omitted, since experimentally it was found to play a negligible role.

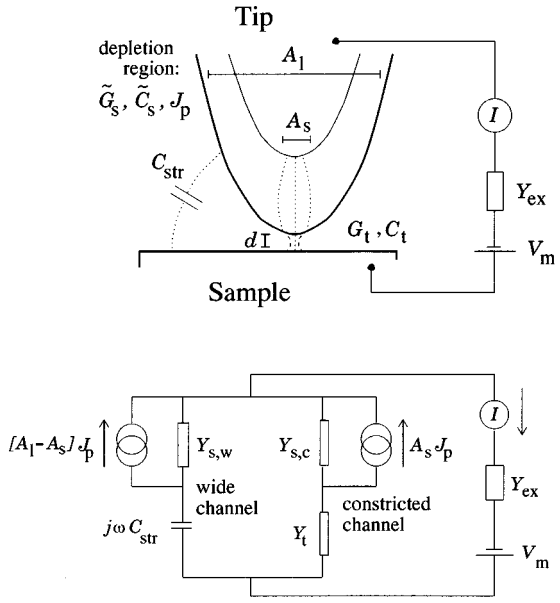

FIG. 5. Electronic model (top) and equivalent circuit (bottom) of an illuminated metal-semiconductor STM junction, where in this case the semiconductor is shaped as a tip. A_l is the illuminated area of the tip. A_s is the section in the semiconductor subsurface region, that is effective for carrier transport toward the tunneling point. The dotted lines represent some relevant electric field lines. See the text for further explanation.

Let us consider a modulation of light intensity ΔP at frequency ω, which imposes a modulation onto the system by means of the following two electronic quantities: a modulation of the photocarrier current ΔJ_p according to Eq. (8), and a modulation of the tunnel barrier conductance ΔG_t due to thermal expansion. Using the equivalent circuit, we calculate the modulation of voltage on the semiconductor surface in the constricted, as well as in the wide channel, and deduce the total detectable current modulation:

$$\Delta I = \underbrace{\frac{Y_t}{Y_t + Y_{s,c}} A_s \Delta J_p}_{\Delta I_{tp}} + \underbrace{\frac{Y_{s,c}}{Y_t + Y_{s,c}} [V_m - V_s] \Delta G_t}_{\Delta I_{tt}} + \underbrace{\frac{j\omega C_{str}}{j\omega C_{str} + Y_{s,w}} [A_l - A_s] \Delta J_p}_{\Delta I_C}. \tag{14}$$

The first term of ΔI is the modulation of constricted current due to photocurrent generation, and will be denoted by ΔI_{tp}. The second term is the modulation of constricted current caused by a modulation of the tunnel barrier conductance, abbreviated by ΔI_{tt}. The third term gives the displacement current through the stray capacitance C_{str} and is called ΔI_C. Note that in practical cases, $\omega C_{\mathrm{str}} \ll |Y_{s,w}|$.

The modulation of tunnel barrier conductance ΔG_t can be caused by thermal expansion of the junction. In this perspective, an important parameter is the distance of thermal diffusion within one modulation period, given by $d_{\mathrm{th}} = [\kappa_{\mathrm{th}}/\omega]^{1/2}$. Here, κ_{th} is the thermal diffusivity that equals approximately $5\times10^{-5}\,\mathrm{m^2\,s^{-1}}$ in GaAs. For the experimentally used modulation frequency of 84 kHz, we find a thermal diffusion length of 10 μm. This is smaller than the typical spot size (20 μm or larger). Therefore, we neglect lateral heat transport and consider the heat conduction to be one dimensional. Then, the modulation of tip-sample separation takes the following simple form:[32]

$$\Delta d = \frac{j\alpha_{\mathrm{th}} f_{\mathrm{th}} \Delta P}{\omega C_p A_l}, \tag{15}$$

where α_{th} is the thermal expansion coefficient, f_{th} takes account of the fraction of incident optical power that is absorbed in the expanding body ($0 \leqslant f_{\mathrm{th}} \leqslant 1$), and C_p is the heat capacity per unit volume. Both tip and sample can exhibit thermal expansion and hence cause a modulation of tip-sample separation. For example, using $\alpha_{\mathrm{th}} = 10^{-5}\,\mathrm{K^{-1}}$, $f_{\mathrm{th}} = 0.3$, $C_p = 10^6\,\mathrm{Jm^{-3}\,K^{-1}}$, and $\Delta P/A_l = 10^5\,\mathrm{Wm^{-2}}$, we estimate Δz to be less than 10^{-12} m at a modulation frequency of 84 kHz. Combining Eqs. (9) and (15), we find that the complex phase of $\Delta G_t/G_t$ is $-\pi/2$, implying that the conductance changes lag the optical power variations.

Finally, we note that in the outlined model the influence of a limited carrier relaxation time of the surface states is not considered. In surface states, electron-hole recombination is generally very fast: in the native oxide on GaAs for example, recombination takes place on a subnanosecond time scale.[16] On the other hand, the cascadelike relaxation process of charges in the surface states can be rather slow if the density of surface states is low or if surface trap states are involved. The proper description by statistical mechanics requires solving the rate equations of the interactions between the surface states, the semiconductor conduction and valence band, and the metallic electrode.[33] A particular difficulty is that detailed knowledge of surface state properties is difficult to obtain. The incorporation of statistical parameters into our model remains to be investigated.

III. EXPERIMENT

The experiments were performed in a STM at ambient temperature and pressure, using GaAs samples as well as GaAs tips. Optical excitation was provided by a linearly polarized single-mode HeNe laser (633 nm). In order to be able to regulate the dc optical power and perform an optical power sweep, the beam was guided through a Pockels cell and polarizer, as depicted in Fig. 6. Subsequently, a photoelastic modulator (PEM), a $\lambda/4$ plate, and an analyzer served to make a relative optical power modulation $\Delta P/P$ at

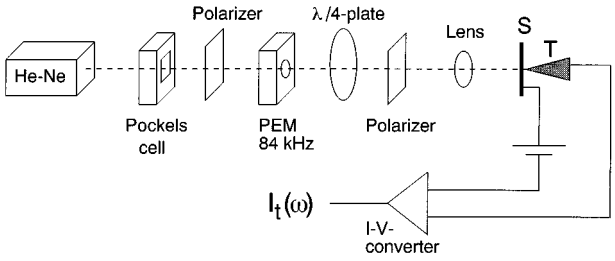

FIG. 6. Experimental arrangement. The STM geometry is indicated for the usage of semiconductor tips (T) and a semitransparent sample (S).

84 kHz. Finally, the beam was focused into the STM junction by a 30-mm focal length objective. In the STM, the spot diameter could be optimized with a relative uncertainty of 25%. Beam deflection due to the Pockels cell or the photoelastic modulator was verified to be negligible. In the STM junction the spot size amounted to a few tens of μm, yielding illumination intensities between zero and $10^6\,\mathrm{Wm^{-2}}$. The estimated[34] local temperature rise was less than 1 K. Semiconductor tips were illuminated along the tip axis through a semitransparent sample (see Fig. 6), consisting of a 20-nm sputter-deposited Pt film on glass. The experiments on semiconductor samples were performed with sharply etched Pt-Ir tips, while illuminating the tunnel junction at about 50° from the sample normal. The GaAs tips and samples were prepared by cleaving polished and epitaxially grown (001) wafers along (110) and (1$\bar{1}$0) directions. The GaAs tips consist of a corner that is bounded by cleavage planes. Inspection by scanning electron microscopy and STM showed that cleavage produces well-defined corners with tip apex radii smaller than 100 nm. When used for topographical imaging in a STM, these tips yield a resolution close to a nanometer under ambient conditions.[8,10] The GaAs was n type (Si doped) or p type (Zn doped), with doping densities ranging from $10^{22}\,\mathrm{m^{-3}}$ to $5\times10^{23}\,\mathrm{m^{-3}}$. The bandwidth of the STM constant-current regulation circuit was set between one and two kilohertz. The STM current was measured by a homemade current-to-voltage converter with a bandwidth of 100 kHz. The data have been corrected for the I-V converter response, which at the highest frequencies could be determined with an accuracy of 10% and a phase uncertainty of about 10°. The signal was fed into a lock-in amplifier to allow for phase-sensitive detection of the current modulation.

IV. RESULTS AND DISCUSSION

In this section, we will present a comparison between experimental results and calculated curves. The latter were established by solving the current conservation rule $I_t = I_s + I_p$, with the equations presented in the previous sections. Except when stated otherwise, it was possible to fit the model calculations to the measurements with a certain range of values for the fit parameters. These values are summarized in Ref. 35. Most experiments presented in this section were performed with semiconductor tips, as well as with semiconductor samples. We could not detect systematic differences between the photoelectrical properties of cleaved tips and

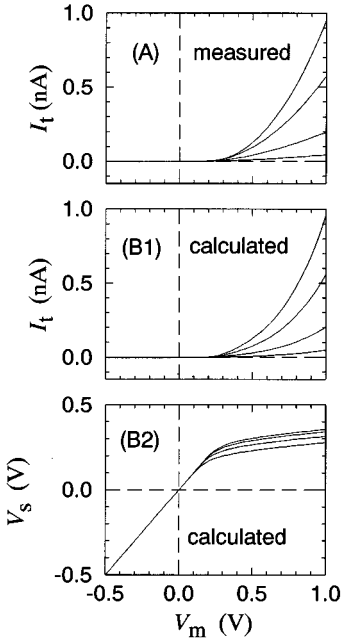

FIG. 7. Measured (a) and calculated (b1) current versus voltage curves, for a nonilluminated GaAs tip (n-type, 2×10^{23} m^{-3} doping density). Panel (b2) shows the surface electrochemical potential V_s that follows from the calculated curves presented in (b1). The curves of panel (a) were measured starting from different set point values for current and voltage. The various calculated curves only differ in the magnitude of the tunnel barrier conductance. Fit parameters are summarized in Ref. 35.

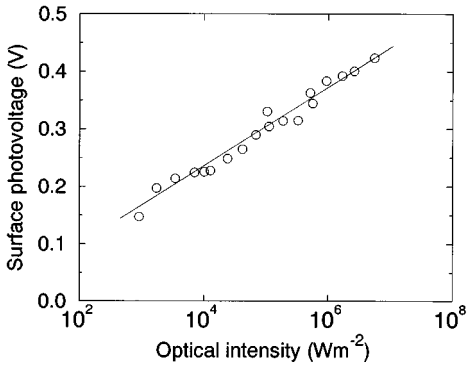

FIG. 8. Measured (symbols) and calculated (line) surface photovoltage versus incident optical intensity for a GaAs sample (p-type, 10^{22} m^{-3} doping density). Fit parameters are summarized in Ref. 35.

planar samples of the same material; apparently, the Schottky barrier properties were more strongly determined by the voltages applied to the junction, than by the shape of the material. In our semiconductor materials the depletion region depth ranges between 50 and 100 nm, so for tips with, at the apex, a radius of curvature of that order, we do not expect to see any differences with respect to a planar material (cf. Sec. II.B.); in case of tips with a far smaller radius of curvature, a possible explanation for our experimental observation is that the cleaved GaAs tips have a very wide tip angle (90°), which suppresses the importance of the radius of curvature for the depletion field profile.

Figure 7(a) shows measured static (so with the feedback-loop turned off) current versus voltage (I-V) characteristics at different set point values for current and voltage, corresponding to different values for the tip-to-sample separation. The indicated data are averages of 225 spectrocopic curves, taken with a GaAs tip in the absence of illumination. Panel (b1) shows calculated current versus voltage curves, where for the different curves only the tunnel barrier conductance was scaled. The top curve with repect to the bottom curve of panel (b1) involved an upscaling of the conductance by a factor of 25. This corresponds to an estimated change of the tip-to-sample separation of 0.5 nm.

At small positive voltages — when the Fermi level of the metallic electrode is positioned within the semiconductor bulk band gap — we observe significant current flow, indicating that carrier flow mediated by surface states occurs. The observed rectification is a result of the pinning action of the surface states, which is well described by the model calculations. At 1 V reverse bias, the current is smaller than 1 pA, indicating that at this point both the Schottky barrier conductance and the surface conductance are lower than $10^{-12}\,\Omega^{-1}$. Since in normal STM operation the junction conductance is of the order of $10^{-9}\,\Omega^{-1}$, this indicates that the surface conductance through the native oxide on GaAs is of negligible magnitude. Panel (b2) shows the calculated surface electrochemical potential (V_s) that follows from the calculations. For $V_m<0$ the Schottky barrier is reverse biased, such that the voltage drop across the Schottky barrier (V_s) equals the externally applied voltage (V_m). At an applied voltage higher than $\sim$0.2 V, the Schottky barrier is sufficiently forward biased to be of comparable or higher conductance than the tunnel barrier, causing the voltage drop across the Schottky barrier to be only part of the applied voltage (V_m).

To further test the applicability of our model, we performed measurements of the SPV versus optical power. As discussed with Eq. (10), the SPV is determined by the zero-current point. Representative results are shown in Fig. 8, showing the expected logarithmic behavior. From the slope of the curve, for $n/[1-\gamma_s n]$ we deduce a value of 1.15 $\pm$0.10 [cf. Eq. (10)]. Actually, this value represents a measurement of n, because γ_s is very small in our system [see the estimates with Eq. (6)]. Because n is close to unity, we conclude that a model based on thermionic emission is indeed applicable. From the model calculation, we deduce that the magnitude of the Schottky barrier height was 0.5 V for this p-type material. The barrier heights determined in this way[35] are in good agreement with the results of other measurement techniques.[14] Due to the higher barrier height of n-type material compared to p-type material, the SPV on the n-type material attains a reasonable value at substantially lower light intensities than needed for the p-type material.

In Fig. 9 we have depicted a set of I-V curves at constant illumination intensity, for n-type GaAs of doping density 2×10^{23} m^{-3}. The top panel (a) shows the measured data, the bottom panel (b) displays calculated curves for different magnitudes of the tunnel barrier conductance. With respect to the nonilluminated case (cf. Fig. 7), the most important differences are the appearance of a surface photovoltage, i.e., a shift of the zero-current point into the higher forward bias direction, and the observation of a considerable current at

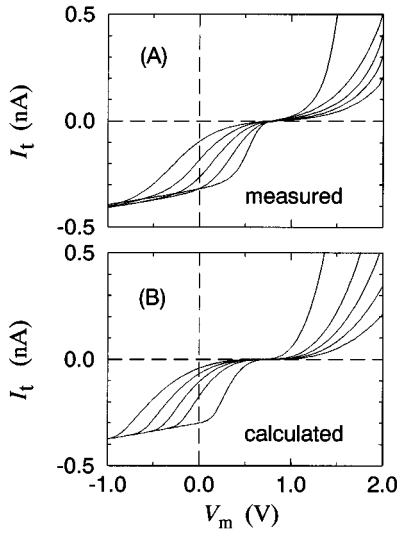

FIG. 9. Measured (a) and calculated (b) current versus voltage curves for an illuminated GaAs tip (n-type, $2\times10^{23}\,\mathrm{m}^{-3}$ doping density). The curves of panel (a) were measured starting from different set point values for current and voltage. For the different curves of panel (b), only the magnitude of the tunnel barrier conductance was scaled. $P/A_l = 10^3\,\mathrm{Wm}^{-2}$. Fit parameters are summarized in Ref. 35.

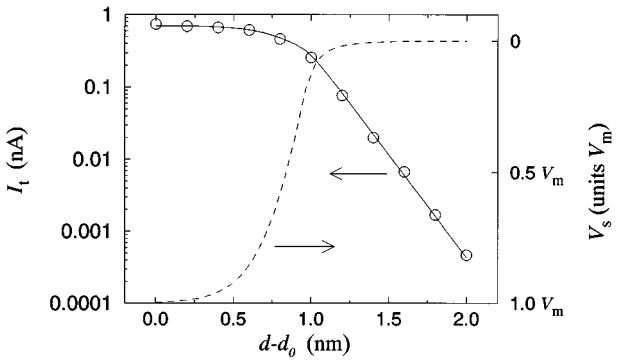

FIG. 10. Tunnel current (left scale) and voltage drop across the Schottky barrier (right scale), as a function of the tip-sample separation (d) relative to the set point at $d=d_0$. For a nonilluminated GaAs tip (p-type, $5\times10^{23}\,\mathrm{m}^{-3}$ doping density). Symbols represent measured points, lines are calculated values. Constant applied voltage $V_m = 0.5$ V. Fit parameters are summarized in Ref. 35.

reverse bias. The SPV is the same for every tip-sample distance, within the experimental accuracy of about 10 mV (see also Refs. 5,10). If the photocarriers that are swept toward the semiconductor surface would not be captured in the surface states, but instead immediately be transmitted into the metallic electrode, the zero-current voltage would depend on the tunnel barrier conductance in a very sensitive way. Since this is not observed, it proves that the carriers are captured in the surface states. In addition, we observe that the curves converge in the reverse bias direction ($V_m<0$). The latter behavior is related to the limited amount of photoexcited carriers that can be collected at the tunnel junction. Qualitatively, we can distinguish a photovoltaic and a photoamperic mode of operation of the semiconductor. The photovoltaic regime occurs in the vicinity of the SPV, when the tunnel current is smaller than the photocarrier current ($\sim$0.3 nA); then, the I-V curves can be described in terms of a nonlinear tunnel conductance connected to a voltage source with a high internal conductance. At reverse bias, we enter the photoamperic regime; this corresponds to a highly loaded semiconductor, operating as a current source with a low internal conductance. In the absence of irradiation, this material does not allow us to drawn a current at reverse bias (cf. Fig. 7); according to Fig. 9, the maximum current at $V_m = 0$ amounts to approximately 0.3 nA at the specified light intensity. Using the equality of Eq. (13), we estimate the collection radius of photogenerated charge to be one μm. This is of the same order as the minority carrier diffusion length in GaAs.[16] It is not surprising that carrier diffusion is of importance, since the optical penetration depth (0.25 μm) is larger than the depth of the band-bending region (0.1 μm at maximum). Note that the size of the saturation current significantly depends on the applied voltage. As was discussed with Eq. (7), the observed increase cannot be simply explained by an increase of the depth of the space charge region. As a possible explanation, we invoke the focusing effect that becomes increasingly pronounced at reverse bias; to account for this effect, in the model calculation we have added a small linear voltage dependence to the effective section A_s. In conclusion, the observed reverse bias current indicates that significant three-dimensional transport of minority carriers (focusing) occurs in the semiconductor subsurface region. The importance of minority carrier focusing by drift (inside the depletion region) versus focusing during diffusive transport (outside the depletion region) cannot be judged at present.

It was pointed out that an illuminated metal-semiconductor STM junction can be operated in two distinct regimes: the photovoltaic regime, when the Schottky barrier conductance is higher than that of the tunnel barrier; and the photoamperic regime, when the Schottky conductance is lower than that of the tunnel barrier. In the previous case (Fig. 9), the transition from one regime to the other is regulated by the bias voltage. Another way to establish the transition is by adjusting the tip-sample separation. Figure 10 depicts a measurement of current versus tip-sample separation (relative scale) for a nonilluminated GaAs tip. By making reproducible topographic scans, it was verified that tip and sample were never in contact. The calculated curves for the tunnel current (left scale) and for the voltage drop across the Schottky barrier (right scale) are also indicated. At high tip-sample separation, an exponential behavior of current versus distance is observed, in agreement with Eq. (9).[36] Using that equation, from Fig. 10 we deduce for κ a value of 3.2 nm^{-1}, which corresponds to an apparent tunnel barrier height ($\hat{\Phi}_t$) of 0.4 V . These are reasonable values for a measurement under ambient conditions.[25] Upon closer approach, the current saturates when the tunneling conductance has become higher than the Schottky conductance; at that point, the Schottky barrier voltage drop equals the externally applied voltage V_m, indicating that the Schottky barrier conductance has become the limiting factor for current conduction.

In a planar solid-state metal-semiconductor junction, the consequence of illumination is that an extra current contribution is added, with a sign independent of the bias voltage V_m: the absolute magnitude of the current increases in re-

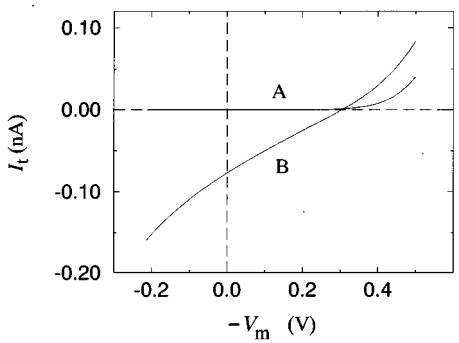

FIG. 11. Current versus voltage curves without (a) and with (b) laser excitation at the same tip-sample separation, for a GaAs sample (p-type, $5\times10^{23}\,\mathrm{m}^{-3}$ doping density). These curves were composed by chopping the light at 4 kHz. In the illuminated situation, $P/A_l=10^5\ \mathrm{Wm}^{-2}$.

verse bias and decreases at a forward bias higher than the SPV. However, in STM experiments with p-type GaAs of moderate or high doping, we have observed a very different behavior in forward bias. An example is depicted in Fig. 11, showing I-V curves taken at the same tip-sample separation. At a forward bias higher than the SPV, upon illumination, the current shows a clear increase, in contrast to the general behavior in planar devices. The estimated[37] increase of the tunnel barrier conductance, due to thermal expansion, was less than 10%. By additionally measuring difference curves at high modulation frequencies (84 kHz), we verified that thermal expansion was not the reason for the observed crossing of the I-V curves.

Our calculations indicate that the direction of the band bending was certainly not reversed by the applied forward bias. Hence, as was pointed out in Sec.II A, in case of a forward bias potential on the semiconductor surface, J_s is of opposite sign compared to J_p. This means that in a forward biased planar junction, an increased illumination can not enlarge the total current density (J_s+J_p) flowing in the semiconductor, and as a result cannot cause an increase of J_t. Qualitatively, the observed behavior can be explained by the fact that the effective section A_s depends on the band-bending profile. As we have discussed in Sec. II B, in the space charge region, the (de)focusing of field lines depends on the relative difference between the band bending at the tunneling point and the band bending away from the tunneling point [represented by the parameter f_1 in Eq. (12)]. Upon irradiating the semiconductor, there is an overall decrease of the depth of the band-bending region (w_0), which according to Fig. 3 gives a weaker defocusing in forward bias $(f_1<0)$. A weaker defocusing implies an increased effective section for charge transport through the Schottky barrier. Hence, when in forward bias the current is mainly determined by the flow of majority carriers, an increased effective section due to illumination gives an increase of the magnitude of the total current. In other words, the fact that curves (A) and (B) of Fig. 11 cross at a certain point, may be a consequence of the (de)focusing properties of the semiconductor band-bending region. At present, we are unable to quantitatively model these effects, because the transport of majority carriers through a nonplanar Schottky barrier has not yet been calculated.

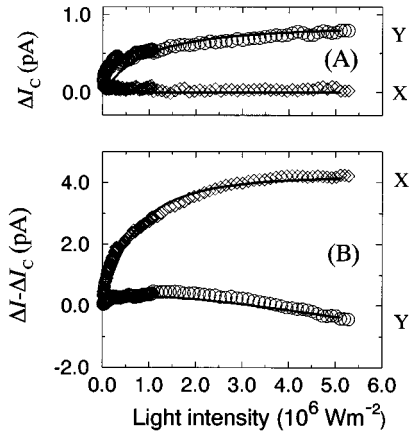

FIG. 12. Measured (symbols) and calculated (lines) phase-sensitive current modulation (x=in-phase, y=out-of-phase) versus incident illumination intensity. The calculated curves are nearly obscured by the data. The top figure (a) shows the current modulation through the stray capacitance, measured while out-of-tunneling at a tip-sample separation of about 0.5 μm. The bottom figure (b) displays the current modulation while tunneling, corrected for the stray capacitance contribution. For a p-type GaAs tip of doping density $5\times10^{23}\,\mathrm{m}^{-3}$. Fit parameters are summarized in Ref. 35. Relative power modulation $\Delta P/P$ = 10% at 84 kHz. Estimated uncertainty of current modulation is 0.2 pA. Set dc tunnel current I=0.5 nA; V_m=0.5 V.

Modulated photoexcitation. From the previous data, we conclude that a semiconductor tunneling tip can be very sensitive to optical excitation, making these tips interesting as scanning local photodetectors[8] and as sources of optically oriented spin-polarized electrons.[9,10] However, because a STM is normally operated in the constant-current mode, the frequency band between zero and about 2 kHz is used for stabilization of the tip-to-sample distance. Hence, additional signals have to be detected at frequencies higher than the bandwidth of the constant-current feedback system. In this perspective, we will study the response of a metal-semiconductor tunnel junction at a frequency of 84 kHz and compare the results to calculations based on the model described in Sec. II C. The model calculations were made by solving the equivalent electrical circuit (cf. Fig. 5) for the constricted as well as for the wide channel, with the aid of an iterative computer code.

The sensitivity of the current to a modulated photoexcitation is depicted in Fig. 12 for p-type GaAs of $5\times10^{23}\,\mathrm{m}^{-3}$ doping density, and in Fig. 13 for n-type GaAs of $2\times10^{23}\,\mathrm{m}^{-3}$ doping density. The measurements were made by sweeping the dc optical power, while keeping the constant-current feedback loop enabled. The relative modulation of incident optical power $\Delta P/P$ was constant during the sweep. The in-phase (x) and out-of-phase (y) current modulations were recorded with a lock-in amplifier. The top panels (a) show the signal detected when the tip was retracted from the sample by $\sim0.5\,\mu$m, i.e., a signal due to stray capacitive coupling between tip and sample only. The bottom panels (b) depict the current modulation measured in tunneling range, when the stray capacitance contribution has been subtracted.

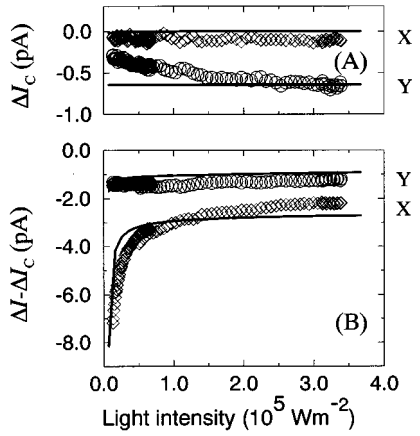

FIG. 13. As Fig. 12, now for an n-type GaAs tip of 2×10^{23} m^{-3} doping density; $V_m = 0$.

Figure 12(a) shows the measured stray capacitance signal when the tip was retracted from the sample by approximately 0.5 μm. The capacitive coupling can clearly be detected[38] and is well described by our model.[39] The model calculation yields a stray capacitance of 0.3 fF (the capacitance reduction factor of Sec. II C is neglected). When corrected for the stray capacitance signal, the measured signal while tunneling contains a photocarrier contribution (ΔI_{tp}) and a contribution due to modulation of the tunnel barrier conductance (ΔI_{tt}) by thermal expansion. As shown in Fig. 12(b), the combined signal contains an in-phase as well as an out-of-phase component (see Ref. 40). The out-of-phase component has a contribution from ΔI_{tp} because Y_t is complex, and a contribution from ΔI_{tt} because ΔG_t (due to thermal expansion) is out of phase at $-\pi/2$. The model calculation takes account of the combined signal, yielding a tunnel barrier capacitance of 0.3 fF. This is the capacitance associated with the approach of the tip to the sample by about 0.5 μm. For the relative tunnel barrier conductance modulation due to thermal expansion, the model calculation yields a value $[\Delta G_t/G_t]/\Delta P = 10\ W^{-1}$. In this experiment the maximum value of ΔP was 0.16 mW. Using these values and Eq. (9) with $\kappa = 3.2\ nm^{-1}$ (cf. Fig. 8), we calculate a corresponding modulation of tip-sample separation of $\Delta d = 0.2$ pm. This is close to the value that was estimated with Eq. (15). Furthermore, the size as well as the phase of the heating signal compare well with a similar measurement using a metallic tip and sample.[7]

As depicted in Fig. 13, the data on modulated photoexcitation in n-type GaAs show a different behavior. This mainly originates from the fact that the Schottky barrier height is larger in n-type than in p-type material.[14,35] As a consequence, the important changes in optical sensitivity occur at lower light intensities, where photothermal effects are still negligible. As shown in Fig. 13(b), at high optical power a rather constant modulation signal is observed, in agreement with our model.[41] The signal phase is nonzero due to the tunnel barrier capacitance. The most striking feature comes in at low light power, when the modulation signal shows a rapid increase. The increase is also observed if a reverse bias is applied to the junction. The reason is that the Schottky saturation current $I_0 = A_s J_0$ is very small for this material, far smaller than the tunnel current. As a result, the semiconductor surface voltage collapses and the tip-sample separation is reduced, when the size of the available photocurrent (I_p) approaches the magnitude of the tunnel current. At that point the photoamperic regime is approached; as expected, we observe that the tunnel current has a maximum sensitivity to variations of the optical intensity toward the photoamperic mode of operation (see also Ref. 6). We were unable to make high-resolution topographic scans in the photoamperic mode of operation, most probably because in that regime the total tunnel current is rather insensitive to variations of the tip-sample distance. Finally, the model calculation for ΔI_C gives a signal of the right size and the right phase; the fact that the calculation does not explain the observed rather weak dependence on optical power remains to be investigated.

In conclusion, for p-type as well as for n-type GaAs tips (i.e., for material with respectively a low and with a high Schottky barrier height) of $\sim10^{23}\ m^{-3}$ doping density, the response of the current to a modulation of optical power can be understood with the model outlined in Sec. II C. The current is composed of signals due to photocarrier modulation, thermal expansion, and due to capacitive tip-sample coupling. For both materials, the signal due to photocarrier modulation saturates at high optical intensities. The sensitivity to optical power is highest for n-type GaAs close to the photoamperic mode of operation.

IV. SUMMARY AND CONCLUSIONS

From the theoretical estimations and a comparison between measurements and calculations, the following picture arises as to the photoelectrical properties of moderately doped GaAs in an ambient STM. First of all, the semiconductor surface states play a crucial role. Not only do the surface states support current flow by strongly communicating with the semiconductor valence and conduction band, they are also effective in shielding the charge on the metallic electrode and in pinning the surface Fermi level. The current-voltage characteristics can be described by considering sequential transport through the serial arrangement of a tunnel and a Schottky barrier. The tunnel barrier is represented by a nonlinear conductance, whereas transport through the Schottky barrier can be described by thermionic emission of majority carriers. As a result, across the Schottky barrier an important drop of electrochemical potential may occur, especially in reverse bias operation. For a given semiconductor, the relative importance of the Schottky versus the tunnel barrier conductance can be tuned by changing the applied voltage or by adjusting the tip-to-sample separation. When optically exciting the semiconductor, an additional minority carrier current is generated in the semiconductor. The voltage that develops on the semiconductor surface is determined by the balance between the majority and minority carrier current in the semiconductor, and the current across the tunnel junction.

The heart of the photoelectrical properties of semiconductors in a STM lies in the understanding of the carrier flow in the semiconductor subsurface region. The tunneling point represents a nanometer-sized constriction of current, but in the semiconductor subsurface region the current density distribution can have a considerably larger lateral extent. The effective section for majority and minority carrier transport

in the semiconductor is determined by the band-bending profile and possible conduction along the surface. For the photoexcited minority carriers, the effective collection radius is estimated by measuring the maximum tunnel current that can be drawn at a certain illumination intensity. This estimation yields a value of one μm for n-type GaAs and a somewhat lower value for p-type GaAs. Since the surface conductance was determined to be negligible, we attribute the measured photocarrier collection area to the nonplanarity of the subsurface carrier flow. As we illustrated with electrostatic calculations, a locally applied reverse potential produces a band-bending profile that acts as a focusing lens for the collection of photoexcited minority carriers. According to our calculations, in the depletion region a focusing power of more than two orders of magnitude is possible. This effect can be enhanced by a focusing effect during the diffusive transport of carriers that are generated outside the depletion region.

The sensitivity of the tunnel current to a modulation of incident optical power was investigated. Good agreement was obtained between the experimental results and the model calculations. The appearance of a modulated surface photovoltage causes direct as well as displacement currents. Also a signal due to thermal expansion was present. Phase-sensitive detection allows for a separation of the different contributions.

To illustrate some consequences of our present understanding, we turn to the application of semiconductor tips for the detection of magnetic sample properties. Magnetic imaging can be achieved in two distinct ways, namely, by magneto-optical near-field imaging[8] and by spin-polarized tunneling due to optical spin-orientation.[9–11] In magneto-optical imaging, the semiconductor tip operates as a local photodetector that maps the polarization-dependent optical properties of a magnetic material. This implies that the main interest is directed toward a small collection volume for photocarriers and a high sensitivity to variations of the optical intensity. In principle, the optical sensitivity of the tunnel current is highest for a material with a high Schottky barrier and a low doping density, operated in the photoamperic mode of operation (when the tunnel barrier conductance is higher than the Schottky barrier conductance). However, this mode of operation is not always convenient, because the tunnel current becomes rather insensitive to changes of the tip-sample separation, which can induce a loss of tunnel junction stability. The requirement of a small collection volume of photocarriers can be achieved by (i) a reduction of the diffusion length (higher doping density, or a different semiconductor material), (ii) a reduction of the optical penetration depth to below the depth of the depletion region (radiation of shorter wavelength), or (iii) a reduction of the focusing power of the depletion field (forward bias operation, or a sharper tip). A possible reduction of the surface photovoltage and of the detectable photocarrier current can be compensated for by increasing the optical power. Special care will have to be taken to avoid signals due to thermal expansion to start dominating, for example, by increasing the modulation frequencies; in turn this may yield a more pronounced contribution of displacement currents.

In a spin-polarized tunneling experiment, the aim is to detect spin-polarized transmission through the tunnel barrier, which means that we should tune the junction to a high sensitivity for tunnel barrier transmission changes. Then, the photovoltaic mode of operation is appropriate, for which the tunnel barrier conductance is lower than the Schottky conductance. Furthermore, it is of interest to obtain a low sensitivity of the tunnel current to variations of the optical power. This can be done by changing the externally applied voltage. Interestingly, for some materials we have observed a working point with the special feature that for a given applied voltage the tunnel current is insensitive to variations of the optical power (cf. Fig. 11).

In conclusion, the presented model gives a good description of the experimentally observed photoelectrical properties of moderately doped GaAs in an ambient STM. The model allows for clear predictions on the applicability of photoexcited semiconductor tips in a STM. For future directions, it would be of interest to study the transition from a high to a low density of surface states, for example, by preparing the semiconductor in an ultrahigh vacuum environment, or by chemically treating the semiconductor surface.[42,43] Furthermore, an improved understanding of the three-dimensional band-bending profile and the majority and minority carrier transport sections is needed. This issue can experimentally be addressed by studying the minority carrier collection area for materials of different doping density and diffusion length. These studies may also reveal the nature of the observed configurations where the tunnel current is insensitive to variations of the optical intensity. Finally, for high-frequency and time-resolved optical STM studies on semiconductors,[44] it will be interesting to establish a statistical model of the electronic interactions between the semiconductor bands, the surface states, and the metallic counter electrode.

ACKNOWLEDGMENTS

We thank J. Hermsen, J. Gerritsen, A. van Etteger and J. van Huet for technical support. A. van Geelen kindly supplied us with semiconductor materials. We thank H. Salemink for critically reading the manuscript. Part of this work was supported by the Stichting Fundamenteel Onderzoek der Materie (FOM), which is financially supported by the Nederlandse Organisatie voor Wetenschappelijk Onderzoek (NWO). The research of R. Groeneveld has been made possible by a fellowship of the Royal Netherlands Academy of Arts and Sciences.

*Present address: Philips Research Laboratories, Prof. Holstlaan 4, 5656 AA Eindhoven, The Netherlands.

[1] A review on STM can be found in *Scanning Tunneling Microscopy I, II, and III*, edited by R. Wiesendanger and H.-J. Güntherodt, Springer Series in Surface Science Vols. 20, 28, and 29 (Springer Verlag, Heidelberg, 1992/93).

[2] R.M. Feenstra, Surf. Sci. **299/300**, 965 (1994).

[3] R. Maboudian, K. Pond, V. Bressler-Hill, M. Wassermeier, P.M. Petroff, G.A.D. Briggs, and W.H. Weinberg, Surf. Sci. Lett. **275**, L662 (1992).

[4] M. McEllistrem, G. Haase, D. Chen, and R.J. Hamers, Phys. Rev. Lett. **70**, 2471 (1993).

[5] M.W.J. Prins, M.C.M.M. van der Wielen, R. Jansen, D.L. Abraham, and H. van Kempen, Appl. Phys. Lett. **64**, 1207 (1994).

[6] M.W.J. Prins, M.C.M.M. van der Wielen, D.L. Abraham, H. van Kempen, and H.W. van Kesteren, IEEE Trans. Magn. **30**, 4491 (1994); M.C.M.M. van der Wielen, M.W.J. Prins, R. Jansen, D.L. Abraham, and H. van Kempen, in *Photons and Local Probes, NATO Advanced Study Institute, Series B: Physics*, edited by O. Marti and R. Möller (Kluwer, Amsterdam, 1995), p. 275.

[7] R.H.M. Groeneveld, M.W.J. Prins, and H. van Kempen, Surf. Sci. **331-333**, 1299 (1995).

[8] M.W.J. Prins, R.H.M. Groeneveld, D.L. Abraham, H. van Kempen, and H.W. van Kesteren, Appl. Phys. Lett. **66**, 1141 (1995).

[9] M.W.J. Prins, D.L. Abraham, and H. van Kempen, J. Magn. Magn. Mater. **121**, 152 (1993); Surf. Sci. **287/288**, 750 (1993).

[10] R. Jansen, M.C.M.M. van der Wielen, M.W.J. Prins, D.L. Abraham, and H. van Kempen, J. Vac. Sci. Technol. B **12**, 2133 (1994).

[11] M.W.J. Prins, R. Jansen, and H. van Kempen, following paper, Phys. Rev. B **53**, 8105 (1996); M.W.J. Prins, Ph.D. Thesis, University of Nijmegen, 1995.

[12] M.S. Sze, *Physics of Semiconductor Devices* (Wiley, New York, 1981).

[13] H.K. Henisch, *Semiconductor Contacts*, International Series of Monographs on Physics No. 70 (Clarendon Press, Oxford, 1984).

[14] E.H. Rhoderick and R.H. Williams, *Metal-Semiconductor Contacts*, Monographs in Electrical and Electronic Engineering No. 19 (Clarendon, Oxford, 1988).

[15] H.H. Wieder, J. Vac. Sci. Technol. **17**, 1009 (1980), and other contributions in this issue.

[16] R.K. Ahrenkiel, in *Minority Carriers in III-V Semiconductors: Physics and Applications*, edited by R.K. Ahrenkiel and M.S. Lundstrom, Semiconductors and Semimetals Vol. 39 (Academic Press, San Diego, 1993), Chap. 2, p. 39 .

[17] We will call n the ideality factor (as in Ref. 14), although some authors prefer to call n the nonideality factor (Ref.13).

[18] In a similar way the dependence of the equilibrium-state barrier height (Φ_s^0) on the electrode work function difference can be described. For clarity this is omitted.

[19] For the case that the density of surface states equals zero, the exact barrier height is calculated in W.J. Kaiser, L.D. Bell, M.H. Hecht, and F.J. Grunthaner, J. Vac. Sci. Technol. A **6**, 519 (1988).

[20] Z.-H. Huang, M. Weimer, and R.E. Allen, Phys. Rev. B **48**, 15 068 (1993).

[21] The minority carrier velocity in the space charge field is scattering limited at a value close to $v \simeq 10^5\ \mathrm{ms}^{-1}$ for GaAs (Ref.12). Thus, the sweep-out time is $\tau_s \simeq w/v \simeq 0.5$ ps when using $w = 50$ nm. Since the recombination lifetime in GaAs is orders of magnitude larger than a picosecond, recombination losses in the space charge region can be neglected.

[22] C.M. Aldao, A. Palermo, and J.H. Weaver, J. Vac. Sci. Technol. A **10**, 493 (1992).

[23] D.E. Aspnes and A.A. Studna, Phys. Rev. B **27**, 985 (1983).

[24] In comparison, for most materials the yield for electron photoemission is lower than 10^{-2} for photon energies in the visible region [W.E. Spicer, *Optical Properties of Solids*, edited by F. Abelès (North-Holland, Amsterdam, 1972), Chap. 10].

[25] C.J. Chen, *Introduction to Scanning Tunneling Microscopy*, Oxford Series in Optical and Imaging Sciences Vol. 4 (Oxford University Press, New York, 1993).

[26] In a STM, the absolute value of the tip-to-sample separation (d) can be estimated as follows. Upon point contact, the conductance is of the order of the quantum conductance ($2e^2/h \simeq 8\times 10^{-5}\ \Omega^{-1}$); in a STM experiment, the tunnel barrier conductance ranges between 10^{-8} and $10^{-10}\ \Omega^{-1}$. Comparing the tunneling junction with the point contact, we deduce that the relative tunnel barrier transmission ranges between 10^{-4} and 10^{-6}. This relative transmission probability is roughly determined by the factor $\exp(-2\kappa d)$ of Eq. (9), where $\kappa = 3.6 \pm 0.4\ \mathrm{nm}^{-1}$ is a typical value under ambient conditions (cf. Fig. 10). With the mentioned range of the experimental transmission probability, we find a tip-to-sample separation of $d = 1.6 \pm 0.5$ nm.

[27] J.G. Simmons, J. Appl. Phys. **34**, 1793 (1963).

[28] C.H. Henry and D.V. Lang, Phys. Rev. B **15**, 989 (1977).

[29] H.C. Card, Solid-State Electron. **18**, 881 (1975).

[30] The free carrier density inside the semiconductor, caused by the tunneling current, can be estimated as follows. Assuming radial current flow inside the semiconductor close to the tunneling point, at a distance r into the semiconductor, the current density is of the order of $J_s \simeq 1\ \mathrm{nA}/r^2$. In case this current density is furnished by surface recombination, at the semiconductor surface the excess carrier concentration becomes $N_{\mathrm{sr}} = J_s/[ev_{\mathrm{sr}}] \simeq 5\times 10^4/r^2$. Since in our experiments the doping density is about $10^{23}\ \mathrm{m}^{-3}$, we deduce that the excess carrier concentration will not affect the band-bending profile at a distance of more than 2 nm from the tunneling point.

[31] M.W.J. Prins and A.P. van Gelder, Physica B (to be published).

[32] S. Grafström, J. Kowalski, R. Neumann, O. Probst, and M. Wörtge, J. Vac. Sci. Technol. B **9**, 568 (1991).

[33] An example of a statistical description of surface states in a nonilluminated Schottky diode can be found in J. Werner, K. Ploog, and H.J. Queisser, Phys. Rev. Lett. **57**, 1080 (1986).

[34] Assuming radial heat conduction through a cone with solid angle Ω, we can estimate the temperature rise at the illuminated spot to be $\Delta T \simeq P/A_l \times \sqrt{\pi A_l}/(\Omega \lambda_{\mathrm{th}})$, where λ_{th} is the thermal conductivity. In GaAs $\lambda_{\mathrm{th}} \simeq 50\ \mathrm{Wm}^{-1}\,\mathrm{K}^{-1}$. Using $P/A_l = 10^6\ \mathrm{Wm}^{-2}$, $A_l = (20\ \mu\mathrm{m})^2$, and $\Omega = \pi/2$, we estimate the temperature rise at the spot to be 0.5 K.

[35] The parameter values used in the model calculations for the GaAs materials are as follows. The Schottky barrier height in the equilibrium state, for n-type material: $|\Phi_s^0| = 0.8 \pm 0.2$ V, and for p-type material $|\Phi_s^0| = 0.4 \pm 0.1$ V . The radius of the effective semiconductor transport section: for n-type material $R_s = 1.1 \pm 0.4\ \mu$m, and for p-type material $R_s = 0.3 \pm 0.2\ \mu$m (in each figure R_s was taken to be constant, except in Fig. 9). The ideality factor: $n = 1.1 \pm 0.1$. The γ factors of Eq. (4): $\gamma_t = 0.1 \pm 0.1$, and $\gamma_s = 0.02 \pm 0.02$ (in each figure the γ factors were taken to be constant). Parameters of fixed magnitude: $C_t = 0.3$ fF, $C_{\mathrm{str}} = 0.3$ fF, $v_r = 10^5\ \mathrm{ms}^{-1}$, $\eta_q \eta_c = 1$, $f_{\mathrm{abs}} = 0.2$, $\beta = 38.7\ \mathrm{V}^{-1}$, $E_{\mathrm{ph}} = 1.96$ eV, and $\epsilon_s = 13$.

[36] In a serial arrangement of a tunnel barrier and a Schottky barrier, the current depends on the tip-sample separation (d) via the change of the tunnel barrier conductance [cf. Eq. (9)] *as well as* via the change of the Schottky barrier height [cf. Eq. (4)], as was also clearly pointed out in Ref. 20, for example. However, the Schottky barrier height is only of importance if the Schottky barrier (instead of the tunnel barrier) is the limiting factor for current conduction, i.e., when V_s is nonzero. In Fig. 10, this

implies that for $d-d_0$ larger than 1 nm, the tunnel current is not determined by the band bending in the semiconductor, but only by the tunnel barrier conductance.

[37] According to Eq. (15), a power modulation of $10^5\,\mathrm{Wm}^{-2}$ at 4 kHz induces a change of tip-sample separation of 0.01 nm, due to thermal expansion (this is an upper limit, because lateral heat transport has been neglected). Using the data in Fig. 10, the mentioned change of tip-sample separation gives a change of the tunnel barrier conductance of less than 10%.

[38] Capacitive coupling of a photoexcited semiconductor tip has also been detected in an atomic force microscope: J. Mertz, M. Hipp, J. Mlynek, and O. Marti, Appl. Phys. Lett. **64**, 2338 (1994).

[39] It follows from the model calculations of Figs. 12 and 13 that — under the specified operating conditions — the following statements are justified. First, it appears that the Schottky capacitance per unit area is of the order of $10^{-3}\,\mathrm{Fm}^{-2}$, and that the Schottky conductance per unit area ranges from $10^4\,\Omega^{-1}\mathrm{m}^{-2}$ at the lowest light intensities, up to $10^7\,\Omega^{-1}\mathrm{m}^{-2}$ at the strongest illumination. Since the modulation frequency was 84 kHz, this implies that the maximum complex angle of $\tilde{Y}_s$ is close to 10^{-2} rad. Hence, we can essentially neglect the Schottky capacitance and assume that $\tilde{Y}_s$ is equal to $\tilde{G}_s$. As a result, the stray capacitance signal is purely imaginary, which served as an additional phase calibration of the measurements. The tunnel barrier capacitance cannot be neglected; at 84 kHz the complex angle of Y_t amounts to a couple of tens of rad. Second, the semiconductor is operated in the photovoltaic regime, i.e., at every point $G_t \ll A_s\tilde{G}_s$. This implies that in sweeping the optical intensity, $\tilde{G}_s$ is the parameter that varies most strongly. In view of the previous considerations, the power dependence of ΔI_C is determined by the factor $\Delta J_p/\tilde{G}_{s,w}$. The value of $\tilde{G}_{s,w}$ follows from the dc solution of the wide current channel: for $J_p < J_0$ the Schottky conductance has a finite value close to $\tilde{G}_{s,w} = \beta A_s J_0$; if $J_p > J_0$, the value of $\tilde{G}_{s,w}$ becomes proportional to P. Thus, we expect ΔI_C to initially increase with increasing P, and to flatten off at higher light intensities.

[40] Taking account of the comments of Ref. 39, the magnitude of the in-phase component essentially behaves as $\Delta I_{\mathrm{tp}} \propto P/\tilde{G}_{s,c}$. This yields a similar power dependence as was discussed for ΔI_C (Ref. 39).

[41] At high optical power, $\tilde{G}_{s,c}$ varies linearly with P. Since $\Delta I_{\mathrm{tp}} \propto P/\tilde{G}_{s,c}$, at high power ΔI_{tp} is constant.

[42] J.A. Dagata, W. Tseng, J. Bennett, F. Schneir, and H.H. Harary, Appl. Phys. Lett. **59**, 3288 (1991).

[43] M. Passlack, M. Hong, E.F. Schubert, J.R. Kwo, J.P. Mannaerts, S.N.G. Chu, N. Moriya, and F.A. Thiel, Appl. Phys. Lett. **66**, 625 (1995).

[44] M.J. Gallagher, T.G. Ruskell, D. Chen, D. Sarid, and H. Jenkinson, Appl. Phys. Lett. **64**, 256 (1994).